

# RSC Advances



This is an *Accepted Manuscript*, which has been through the Royal Society of Chemistry peer review process and has been accepted for publication.

*Accepted Manuscripts* are published online shortly after acceptance, before technical editing, formatting and proof reading. Using this free service, authors can make their results available to the community, in citable form, before we publish the edited article. This *Accepted Manuscript* will be replaced by the edited, formatted and paginated article as soon as this is available.

You can find more information about *Accepted Manuscripts* in the [Information for Authors](#).

Please note that technical editing may introduce minor changes to the text and/or graphics, which may alter content. The journal's standard [Terms & Conditions](#) and the [Ethical guidelines](#) still apply. In no event shall the Royal Society of Chemistry be held responsible for any errors or omissions in this *Accepted Manuscript* or any consequences arising from the use of any information it contains.

**Visible light Photocatalytic Degradation of Wattle extract: Effect of mixing CdWO<sub>4</sub> over Semiconductive ZnO Photocatalyst**

*E. T. Deva Kumar<sup>1</sup>, K. Thirumalai<sup>3</sup>, R. Aravindhan<sup>2\*</sup>, M. Swaminathan<sup>3</sup>, J. Raghava Rao<sup>1\*</sup>, B. U. Nair<sup>1</sup>*

*<sup>1</sup>Chemical Laboratory, CSIR – Central Leather Research Institute, Chennai, India.*

*<sup>2</sup>Leather Processing Division, CSIR – Central Leather Research Institute, Chennai, India.*

*<sup>3</sup>Department of Chemistry, Annamalai University, Annamalai Nagar, India.*

---

\*Authors for correspondence. email: (J. Raghava Rao) [clrichem@mailcity.com](mailto:clrichem@mailcity.com);  
( R Aravindhan) [aravindhanr78@gmail.com](mailto:aravindhanr78@gmail.com) Tel: + 91 44 2441 1630; Fax: + 91 44 2491 1589)

## Abstract

Wattle (*Acacia mearnsii*) extract, a leather tanning agent which mainly composed of poly – phenolic compounds was tried to degrade by photocatalytic degradation which is a hindrance to the conventional bio - treatment of tannery effluent. To serve the process a novel semiconductive mixed catalyst CdWO<sub>4</sub>-ZnO was prepared by simple hydrothermal method. The degradation reaction was carried with visible light source in neutral medium for three hours duration. The results depicted the better catalytic activity of CdWO<sub>4</sub>-ZnO (band gap 2.8 eV) in degrading the organics when compared to undoped ZnO (band gap 3.8eV) under visible light. The results also showed that the catalyst is appropriate at 36.8 weight percentage of CdWO<sub>4</sub> in ZnO. The catalyst morphological, optical characters and degradation of wattle were carefully analyzed.

**Keywords:** CdWO<sub>4</sub> – ZnO, Visible light photocatalyst, Wattle extract, COD.

## 1. Introduction

Tanneries, which extensively uses various chemicals, discharge millions of liters of waste water with hazardous pollutants <sup>1,2</sup>[1,2]. The materials used in tanning processes are tanning agents, synthetic tanning agents, oil emulsions (fatliquors) and dyes. Conventionally, the effluent from the tannery is treated by means of biological methods, where micro organisms play a vital role in degrading these chemicals <sup>3,4</sup>. The biological treatment methods are not very efficient in treating effluent containing polyphenolic compounds, since polyphenolic compounds react with the microbes through hydrogen bonding and prevent the metabolic activity of the microbes <sup>5</sup>. Hence, there is a need to find alternative solutions for treating the polluted water from tannery units. In recent years, heterogeneous photocatalysis, one of the advanced oxidation processes is used to degrade any kind of organic pollutants in air and liquid <sup>6,7,8,9</sup>. In this work, an attempt has been made for the first time to use semiconductor photo catalyst to degrade wattle bark extract, a constituent of tannery effluent.

Wattle extract is a powder from the bark of the wattle tree (*Acacia mearnsii*). They are natural polymers of polyphenolic compounds and are used as tanning material owing to the presence of larger quantity of condensed tannin. The proanthocyanidine group in wattle extract, which has catechin and gallo catechin starter units and fisetinidol extender units <sup>10</sup> form hydrogen bond with leather making protein (collagen) in the skins and hides <sup>11</sup>, thus it stabilizing collagen and resulting in quality leather. Around four lakh tons of vegetable tannin is being used worldwide for this purpose and almost 60,000 to 80,000 tons of vegetable tannins are let out as spent vegetable tanning effluents annually <sup>12</sup>. The polyphenol compounds in the wattle extract are of environmental concern. The larger amounts of organic compounds causes elevated dissolved organic carbon into the environment, and are hardly biodegradable compounds <sup>13</sup> and also cause

health related issues in human <sup>14</sup>. These effluents are not completely degraded in aerobic biological treatment systems. It also contains non-tannin materials like sugary matter, gallic acid, soluble mineral salts and other organic acids <sup>15</sup>. Reports are available on treatment of these effluents with chemical oxidation processes such as Fenton's process and Ozonation <sup>16</sup> but to our knowledge there are no reports on the treatment of the leather industry waste water with semiconductor photocatalytic process.

Photocatalysis is a type of advanced oxidation process, where the organics are non-selectively oxidized <sup>17</sup>. Photocatalysis finds its application in many fields such as water purification <sup>18</sup>, disinfections <sup>19</sup>, tissue engineering <sup>20</sup>, organic synthesis <sup>21</sup> etc. Generally, metal oxide semiconductors are used as photocatalyst because of their favorable band gap and electronic structures <sup>22</sup>. The semiconductors have a special advantage over the conductors because the band gap between the valence band and the conduction band can be finely tuned according to our interest <sup>23</sup>. Usually, metal oxides like titanium dioxide and zinc oxide are used for heterogeneous photocatalytic degradation reactions, since both of them have band gap values of 3.2 eV. The charge carriers created on the onset of light irradiation react with the organic substances and degrade them by adopting redox reactions <sup>24</sup>. One of the barriers in the degradation reaction is the recombination of charge carriers <sup>25, 26, 27</sup>. For an effective photocatalytic reaction there must be prevention of these charge carrier recombination for considerable time interval <sup>28, 29, 30</sup>. One of the main draw backs with ZnO photocatalyst is faster recombination of charge carrier. To prevent this charge carrier recombination, doping of semiconductor is adopted, where some amounts of foreign material is added as impurities <sup>31, 32</sup>. This will create a hetero junction at the band gap and prolong the time lag between the charge carrier recombination; the doping may also finely tune the band gap of the catalyst <sup>33</sup>. Other method to fulfill this need is the preparation

of mixed semiconductor catalyst with oxides like  $\text{Bi}_2\text{O}_3$ <sup>34</sup>,  $\text{BiVO}_4$ <sup>35</sup>,  $\text{BiPO}_4$ <sup>36</sup>,  $\text{Cu}_2\text{O}$ <sup>37</sup>,  $\text{V}_2\text{O}_5$ <sup>38</sup>. In such mixed oxide catalyst, the stoichiometry of the oxides and the surface structure of the catalyst play a major role in the activity of the catalyst<sup>39</sup>.

Several mixed oxide catalyst with ZnO is found in the literature to degrade the organic dyes some of them are  $\text{TiO}_2\text{-ZnO}$ <sup>40</sup>,  $\text{WO}_3\text{-ZnO}$ <sup>41</sup>,  $\text{ZnO-SnO}_2$ <sup>42,43</sup> the present work, semiconductive mixed oxide catalyst is prepared with zinc oxide and cadmium tungsten oxide nanoparticles. This newly prepared catalyst  $\text{CdWO}_4\text{-ZnO}$  has band gap well below that of bare ZnO viz., 3.2 eV, and hence is active under visible region in neutral medium. This catalyst was employed in the degradation of wattle extract by semiconductive photo catalysis under visible light (400-800 nm) which is 44-47% of the solar spectrum.

## 2. EXPERIMENTAL SECTION

### 2.1. Materials

Sodium tungsten oxide dihydrate, cadmium nitrate, zinc nitrate hexahydrate used for the preparation of catalyst were of analytical grade. Wattle extract powder used was procured commercially. All other chemicals employed in analysis were of analytical grade and used without any further purification. All the solutions were made using double distilled water.

### 2.2. Preparation of $\text{CdWO}_4\text{-ZnO}$

The mixed oxide catalyst was prepared by adopting a hydrothermal procedure. Known quantity of (1.649 g)  $\text{Na}_2\text{WO}_4 \cdot 2\text{H}_2\text{O}$  was dissolved in 100 ml of deionized water and stirred vigorously. To this solution, 1.182 g of  $\text{Cd}(\text{NO}_3)_2$  was added and the stirring was continued. The pH of this solution was adjusted to 10 with NaOH. This resulted in complete precipitation of  $\text{CdWO}_4$ . The

CdWO<sub>4</sub> slurry was added to 100 mL of 0.4 M (Zn(NO<sub>3</sub>)<sub>2</sub>·6H<sub>2</sub>O) solution and stirred for 30 min. Then, 100 mL of oxalic acid in distilled water (0.6 M) was added to the above solution drop wise and stirred for 4 h to ensure complete precipitation of zinc oxalate. A mixed precipitate of zinc oxalate and CdWO<sub>4</sub> was transferred to the teflon lined stainless steel autoclave for hydrothermal treatment at 115°C for 12 h. The pressure was maintained at 18 psi. The mixed precipitate was then dried in air at 90°C for 12 h and calcined at 450°C for 12 h in a muffle furnace to obtain 36.8wt% of CdWO<sub>4</sub> in ZnO.

### 2.3. Instrumentation and Characterization of the catalyst

Surface characteristics including growth, orientation, porosity, structure, and particle size were analyzed by field emission SEM Studies, performed using Hitachi model S3000-H SEM. EDS analysis was performed on gold coated samples with FE-SEM (Model ULTRA-55). HR-TEM images were taken from 200 kV Ultra High Resolution Transmission Electron Microscope (JEOL-2010) having high resolution optical microscope (Leica microscope). XRD was used to identify the crystalline nature and crystal planes associated with the formation of CdWO<sub>4</sub>-ZnO catalyst. XRD studies were carried out using XPERT-PRO multipurpose X-ray diffractometer procured from The Netherlands using Cu K $\alpha$  radiation with a wavelength of 1.540Å and the 2 $\theta$  value was varied from 10° to 80°. The optical properties of the prepared CdWO<sub>4</sub>-ZnO catalyst and ZnO were analyzed using UV-Visible spectroscopy in reflectance mode. These studies were carried out by varying the wavelength from 200 to 1100nm. The UV-Visible analysis in diffuse reflectance mode was performed using Perkin Elmer Lambda 650 UV-Vis spectrophotometer attached with 60mm integrated sphere detector module. The surface morphology and root mean square (RMS) surface roughness of the semiconductor oxides were examined with Nanoscope E (Digital instruments Inc, Model: NSE, USA) atomic force

microscope (AFM) in contact mode using  $\text{Si}_3\text{N}_4$  cantilever. Photoluminescence studies were carried out on a Perkin Elmer LS 55 fluorescence spectrometer. The excitation wavelength used to record PL was 305 nm. The specific surface areas of the samples were determined through nitrogen adsorption at 77 K on the basis of the BET equation using a Micrometrics ASAP 2020 V3.00 H. EPR analysis to find the radicals was done with Bruker EMX plus with microwave frequency of 9.861376 GHz at room temperature. XPS analysis to find the chemical nature of the surface species was done in XM 1000 Omicron nanotechnology machine with  $\text{Al-K}\alpha$  radiation.

#### **2.4. Photo reaction in visible light reactor**

The degradation of wattle with the mixed photocatalyst,  $\text{CdWO}_4\text{-ZnO}$  was carried out in the visible light photoreactor supplied by Heber Scientifics, India. Tungsten lamp (150 W), which covers wavelength range from 400 to 760 nm was used as a light source in the photoreactor and was kept immersed in a quartz tube at the centre of reaction vessel. In all the reactions 50 ml of 1% wattle extract solution and 150 mg of 36.8 wt% of  $\text{CdWO}_4$  in ZnO semiconductor was used as catalyst. The reaction vessel was supplied with atmospheric air by means of air motor pump, which provided necessary oxygen for the reaction. Initially, dark reaction was carried out for 30 minutes with continuous purging of air into the reactor, this action ensure thorough mixing of the catalyst with reaction solution, also the dark reaction aids adsorption of the wattle over the catalyst surface. After dark reaction, light source was switched on. The outer jacket of the reactor was supplied with cold water for cooling purpose throughout the reaction time. The photocatalytic degradation of the wattle was carried out for three hours. An aliquot of 1 mL was collected from the reactor at an interval of every 30 minutes with the help of syringe and analyzed further. The degradation of organics in the wattle by semiconductor photocatalytic

process was examined by measuring the chemical oxygen demand (COD) as per standard procedure APHA (1998) section 5220.

### 3. RESULTS AND DISCUSSION

#### 3.1 SEM analysis

The FESEM images of the mixed catalyst  $\text{CdWO}_4\text{-ZnO}$  prepared by hydrothermal method is shown in Fig.1. The images 1(a, b and c) show the catalyst in different magnifications, viz. 20 K, 40 K and 80 K, respectively. It could be clearly observed from the figures that the catalyst is a nanocomposite and there are mixed combinations of nanospheres and nanoflakes. The size of the nanoparticles formed fall in the range of 60 nm and the heterostructure of the mixed catalyst is clearly depicted in Fig 1c. It is reported that the heterostructure formation at the interfaces between  $\text{CdWO}_4$  and  $\text{ZnO}$  causes redistribution of electric charges across the semiconductor interface and there will be a formation of Schottky barrier, this in turn serves as an electron trap and prevent the charge carrier recombination and increase the efficiency of the catalyst, further this will provide large active sites for the adsorption of foreign substances<sup>44</sup>. Also is observed that the mixed catalyst has a highly porous structure, which enhances the surface area of the catalyst.

#### 3.2. TEM and HRTEM analysis

The heterojunction and fine structural details of the prepared catalyst  $\text{CdWO}_4\text{-ZnO}$  was analysed by means of TEM experiment equipped with HRTEM and SAED facilities. Fig. 2 (a) show the transmission electron micrograph of the mixed oxide at 50 nm scale, where the clear picture of nanostructures are visible. The intercrossing of the mixed catalyst was explored by contrast variations in the image. Fig (2)b shows the HRTEM image of the catalyst at a particular point

where the formation of heterojunction is obvious. The spacing between the adjacent fringes of ZnO is shown to be 0.256 nm which is close to the d spacing of (002) plane in ZnO also the spacing between the fringes of CdWO<sub>4</sub> is found to be 0.3 nm which is also consistent with the inter planar distance of (111) plane in pure monoclinic phase of well-crystallized CdWO<sub>4</sub> with a wolframite structure<sup>45</sup>, moreover the fringes of both CdWO<sub>4</sub> and ZnO is continuous confirming the chemical bond between the two metal oxide structures. Fig 2(c) shows the SAED pattern of the mixed oxide catalyst which confirm the crystalline nature of CdWO<sub>4</sub>-ZnO.

### 3.3. Elemental mapping and EDAX of CdWO<sub>4</sub>-ZnO

To confirm the composition and distribution of Zn, Cd, W, and O in the surface of the mixed oxide catalyst CdWO<sub>4</sub>-ZnO, elemental mapping was carried out. Fig. 3(a) shows the FESEM elemental color composition of CdWO<sub>4</sub>-ZnO. Fig. 3(b), (c), (d) and (e) display the elemental mapping of constituent individual elements, viz., oxygen, zinc, cadmium and tungsten respectively. It is evident that O (Fig. 3b) and Zn (Fig. 3c) are higher in density when compared with Cd and W and there is also a homogenous distribution of Cd, W, Zn and O (Fig. 3a) in the mixed oxide catalyst CdWO<sub>4</sub>-ZnO. It also indicates the purity of the catalyst CdWO<sub>4</sub>-ZnO. Fig. 3(f) shows the EDX spectrum recorded from the selected area reveals the presence of Zn, Cd, W and O in relative composition appropriate for the formation of CdWO<sub>4</sub>-ZnO.

### 3.4. XRD studies

The crystalline structure and phase purity of undoped ZnO and mixed catalyst CdWO<sub>4</sub>-ZnO was analyzed by X-ray diffraction studies. Fig. 4(a) displays the diffraction peaks of ZnO at 31.77°, 34.49°, 36.24°, 56.60°, 62.85°, 66.38°, 67.94°, 69.08°, 72.50°, and 76.93° corresponding to 100,

002, 101, 110, 103, 220, 112, 201, 004, and 202 diffraction planes of ZnO wurtzite structure, respectively. (JCPDS file no. 36-1451)<sup>46</sup> Fig. 4(e) reveals the peaks for a pure monoclinic phase of well crystallized CdWO<sub>4</sub> with a wolframite structure (JCPDS NO. 14-0676). The distinctive peaks at 23.3°, 29.0°, 29.6°, 30.5°, 35.4°, 35.7° and 47.6° match well with 110, -111, 111, 020, 002, 200 and 220 crystal planes of CdWO<sub>4</sub> (Fig. 4d), which is consistent with the results of Ye *et al*<sup>47</sup> An increase in the concentration of CdWO<sub>4</sub> in the catalyst increases the peak intensity of 110, -111, 111, 020, 002, 200 and 220 diffraction planes corresponding to CdWO<sub>4</sub> in ZnO material, this was shown by the diffraction patterns in Fig. 4(b), which is 8.1 wt% of CdWO<sub>4</sub> in the mixed catalyst CdWO<sub>4</sub>-ZnO and Fig 4(c) 23.7 wt% of CdWO<sub>4</sub>.

### 3.5. XPS Analysis

X-ray photoelectron spectroscopy was performed for the prepared mixed oxide catalyst CdWO<sub>4</sub>-ZnO to analyze the different oxidation states and chemical composition of different compounds formed. Fig 5(a) shows the survey scan for the catalyst where the presence of cadmium, zinc, tungsten, and oxygen is evident. The survey also shows the peak for carbon which may adsorb during the exposure to atmospheric air (adventitious carbon). The fig.5(b) shows the high resolution peak for adventitious carbon where the C 1s peak at 284.6 eV is obvious. Fig.6. shows the high resolution peak analysis of individual elements in the catalyst. Fig. 6(a) shows the spin orbital splitting of Cd 3d peak, the Cd 3d<sub>5/2</sub> peak arises at 404.4 eV and the Cd 3d<sub>3/2</sub> peak at 405.2 eV, the peak difference between the two spin orbital splitting peak is 6 eV<sup>48</sup> from which the Cd<sup>2+</sup> chemical nature is confirmed. Fig 6(b) display the peak splitting details for tungsten 4f orbital, the W 4f<sub>7/2</sub> orbital splitting peak arises at 34.9 eV and the W 4f<sub>5/2</sub> splitting comes at 37.0 eV. The difference between the two 4f orbital splitting is 2.18 eV which confirms the presence of W(VI)<sup>49</sup>. Fig.6(c) shows the peak splitting for Zn 2p orbital where the Zn 2P<sub>3/2</sub> arises at 1021.04

eV and Zn  $2P_{1/2}$  peak arises at 1044.25 eV, the difference between the splitting confirms the presence of zinc in divalent state. Fig.6(d) shows the high resolution peak for Oxygen 1s orbital.

### 3.6. AFM Measurements

The surface profile and growth of  $CdWO_4$ -ZnO were analyzed through AFM measurements. The measurements were performed on the  $CdWO_4$ -ZnO coated glass slides. Fig. 7(a) and (b), display representative topography and 3D views of the prepared mixed catalyst  $CdWO_4$ -ZnO, respectively. AFM images of a  $3 \times 3 \mu m^2$  region of  $CdWO_4$ -ZnO reveal its uniform surface morphology. The existence of nanosized particle and porous structure are also evident. The 3D image of the catalyst shows the growth pattern of the crystalline structure, where the height varies from 30 to 60 nm. Moreover, the AFM micrographs clearly demonstrate the formation of highly ordered and porous structure. Further, the root mean square (RMS) roughness of the  $CdWO_4$ -ZnO has been measured to be 8.23 nm. Lv *et al* have reported that films with high specific surface area and improved crystallinity have increased of photocatalytic activity.

### 3.7. Photoluminescence study

The photoluminescence study was carried out for both undoped ZnO and mixed catalyst ( $CdWO_4$ -ZnO). The separation and recombination of the charge carriers is related to the photocatalytic activity of the catalyst<sup>50</sup>. Fig.8 displays the PL spectra of the ZnO and  $CdWO_4$ -ZnO, where the emission band at 418 nm corresponds to the electron and hole recombination in ZnO<sup>51</sup>. The decrease in the PL emission intensity in case of  $CdWO_4$ -ZnO than that of ZnO implies the electron transfer from the conduction band of ZnO to interface of the semiconductors. The generated electron in the conduction band of ZnO by the shine of light is

transferred to the conduction band of CdWO<sub>4</sub>. This action of electron transfer is faster than the recombination of electron with the holes in the valence band, this is facilitated because of lower energy state of CdWO<sub>4</sub>. Thus owing to the pronounced quenching of electron and hole pairs in mixed catalyst, the catalytic activity is increased<sup>52</sup>.

### 3.8 N<sub>2</sub> Adsorption study

The pore structure of the CdWO<sub>4</sub>-ZnO photocatalyst has been investigated by nitrogen adsorption-desorption isotherms and the pore size distribution has been calculated by Barrett–Joyner–Halenda (BJH) method. The N<sub>2</sub> adsorption/desorption isotherms of the synthesized CdWO<sub>4</sub>-ZnO (Fig. 9) exhibit a type III isotherm with a H3 hysteresis loop according to the classification of IUPAC<sup>53</sup>. A sharp increase in adsorption volume of N<sub>2</sub> has been observed and is located in the  $P/P_0$  range of 0.8-0.99. This sharp increase can be attributed to the capillary condensation, indicating good homogeneity of the sample and macro pore size since the  $P/P_0$  position of the inflection point is related to the pore size<sup>54</sup>. Average pore radius of CdWO<sub>4</sub>-ZnO is found to be 325 Å. The pore size distribution of the catalyst confirms a macroporous structure. It could be observed from the BET surface area measurements that the specific surface area of CdWO<sub>4</sub>-ZnO is 24.2 m<sup>2</sup>g<sup>-1</sup>, which is 2.1 times higher than that of ZnO (11.5 m<sup>2</sup>g<sup>-1</sup>).

### 3.9. UV-Visible Diffuse reflectance spectroscopy

The optical properties of the undoped ZnO and mixed catalyst CdWO<sub>4</sub>- ZnO have been analyzed by UV-Vis diffuse reflectance spectroscopy. Fig. 10 (a) and (b) show the UV-Vis spectra of ZnO and the prepared mixed catalyst, respectively. It could be observed from the spectra that the undoped ZnO metal oxide displays a maximum reflectance throughout the visible region (400nm-800nm). In contrast the mixed semiconductor metal oxide (CdWO<sub>4</sub>-ZnO) displays a

distinct change where the reflectance values are comparatively lower than that of undoped ZnO. keen analysis shows that CdWO<sub>4</sub>-ZnO catalyst has higher absorption in visible region than the undoped ZnO. This reveals that the CdWO<sub>4</sub>-ZnO catalyst can be used as a better catalyst in visible region. The band gap values are determined from these spectra by converting the absolute reflection values to Kubelka-Munk function <sup>55</sup>  $F(R_{\infty})$ . The plot between the modified Kubelka-Munk function  $[h\nu F(R_{\infty})]^{1/2}$  versus the energy of absorbed light  $E$  in electronic volts gives the band gap energy of the semiconductors. The values are determined to be 3.2 eV for ZnO and 2.8 eV for CdWO<sub>4</sub>-ZnO mixed catalyst.

### 3.10. IR spectroscopic studies

The functional groups present in the wattle before and after photocatalytic degradation has been analyzed using IR spectroscopy technique. Fig. 11 (a) and (b) show the IR spectra of wattle extract before and after degradation with the CdWO<sub>4</sub>-ZnO catalyst, respectively. The prominent peak in Fig. 11 (a) at 5400 cm<sup>-1</sup> shows the presence of O-H stretching of intra molecular hydrogen bond in the polymeric compound. The peak at 1200cm<sup>-1</sup> is for the presence of C=C-C catenation in aromatic ring system. The presence of a peak at around 2900 cm<sup>-1</sup> is due to stretching of C-H bond. The peak around 1280 cm<sup>-1</sup> is characteristic of flavonoid based tannins. The peak around 900 cm<sup>-1</sup> is for the C-H in plane bending. When analyzing the IR spectra for the wattle extract degraded with the advanced oxidation process the peak around 1600 cm<sup>-1</sup> diminishes, which supports the degradation of aromatic system.

### 3.11. Photocatalytic Degradation in the Visible light reactor

The photocatalytic degradation of wattle was carried out in visible light reactor under neutral pH condition. A tungsten lamp of 150 W has been used as light source. The degradation reaction has

been carried out with 50 mL of 1% wattle solution with 50, 100 and 150 mg of CdWO<sub>4</sub>-ZnO and undoped ZnO catalyst, respectively. Initially, a dark reaction has been carried out for 30 min, followed by light reaction for 3 h. Fig. 12 shows the plot between the percentage reduction in COD and time while using the mixed oxide catalyst ZnO-CdWO<sub>4</sub> which is an estimate of degradation of wattle extract and Fig. 13 shows the degradation of wattle extract using undoped ZnO. It is quite evident from the figures that the CdWO<sub>4</sub>-ZnO catalyst has degraded the wattle to an extent of 48.2% because there is a formation of heterojunction in the mixed oxide catalyst which leads to the formation of electric field at the interface, this prevents the recombination of charge carriers, moreover the band gap of the CdWO<sub>4</sub>-ZnO catalyst at the interface is 2.8 eV which falls well within the visible region and makes the photodegradation an efficient one with the mixed oxide catalyst whereas in undoped ZnO catalyst the recombination of charge carriers is prevalent and also this comes under activity of UV radiation which is very little part of whole spectrum hence it has degradation efficiency of only 20%. The reaction with the 50 and 100 mg of catalyst shows degradation efficiency of 21.43% and 40%, respectively. The degradation reaction also experimented with the mechanical mixing of the two semiconductors which resulted in 20.8% of COD reduction which suggest the formation of chemical bonds between the two oxides and alignment of band structure. The mixed oxide catalyst after the degradation reaction was washed completely with water and applied for fresh reaction for three consecutive reactions the percentage of degradation for 150 mg of catalyst remains around 43%.

### 3.12. Kinetic analysis of the degradation reaction

The kinetic details of the photocatalytic degradation of 1% wattle with bare ZnO and mixed oxide catalyst CdWO<sub>4</sub>-ZnO were analysed using well known Languir-Hishelwood kinetic model<sup>56</sup>, where the equation is modified to the reaction occurring on the solid-liquid interface.

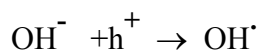
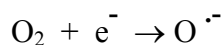
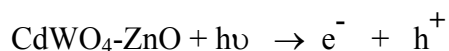
$$r_0 = dc / dt = k_r K C_{eq} / 1 + K C_{eq}$$

where  $r$  is initial rate of degradation reaction,  $K_r$  the rate constant of the reaction,  $K$  adsorption equilibrium constant and  $C_{eq}$  equilibrium concentration of the wattle in the reaction vessel. Fig.14 (a) display the plot of  $C/C_0$  ( $C$  is initial concentration of wattle after attaining the equilibrium with the catalyst and  $C_0$  concentration at the particular time) versus time for three different amount of the mixed oxide catalayst. It is evident from the plots the reaction pathway with 150 mg and 100 mg of catalyast follow zero order reaction kinetics, moreover the 150 mg of  $CdWO_4-ZnO$  catalyast with 36.8 wt % of  $CdWO_4$  shows the highest catalytic activity in degrading the wattle. It is also known from the literature that the photocatalytic degradation of organic pollutants follow the zero order reaction kinetics<sup>57</sup> which indicates that the reaction does not depend on the concentration of the pollutant but the reaction completely depend on the electron-hole recombination rate on the heterogeneous catalys. The fig.14(b) shows the kinetic details of bare ZnO catalyast in degrading the wattle here too the higher amount of catalyast follows the zero order reaction obeying the equation  $C/C_0 = 1 - (K / C_0) t$ . The rate constant for degradation reaction with 150mg of  $CdWO_4-ZnO$  is  $2.67 \times 10^{-3} \text{ mg L}^{-1} \text{ s}^{-1}$  and for bare ZnO is  $1.19 \times 10^{-3} \text{ mg L}^{-1} \text{ s}^{-1}$ . It is also learnt from the plots that both the mixed oxide catalyast and bare ZnO at lower amount i.e at 50 mg /50 ml deviates from the linearity and seems to falls under first order reaction.

### 3.13. ESR study for ZnO and $CdWO_4-ZnO$

It is know from the above experimental evidences that the mixing of 36.8% of  $CdWO_4$  with ZnO enhances the photocatalytic activity of the ZnO in degradation of Wattle due to enhanced charge separation. In the aim of showing the enhanced charge separation and catalytic activity of ZnO

after mixing with CdWO<sub>4</sub>, ESR spectroscopic analysis was performed for the bare and mixed catalyst at room temperature before and after irradiation to ultraviolet radiation. Fig. 15 shows the ESR spectra of (a) bare ZnO before irradiation (b) bare ZnO after irradiation (c) mixed oxide catalyst CdWO<sub>4</sub>-ZnO before irradiation and (d) mixed oxide catalyst CdWO<sub>4</sub>-ZnO after irradiation, the inset graph shows their corresponding g values. Fig. 15(a) display the g value for defects in ZnO and for shallow donors<sup>58</sup> in the ZnO lattices round 1.96 g and it is observed in the fig. 15(b) that there is no change in the defects or vacancies but there is an observation of chemisorbed oxygen. After mixing CdWO<sub>4</sub> with ZnO there is a formation of heterojunction and this will decrease the number of surface vacancies and defects<sup>59</sup>, this is shown in fig 15(c) where the signal due to Zinc defect is not attributed also in fig 15(d) the strong resonance for paramagnetic character around 2.019 g is observed which may due to the O<sup>2·-</sup> radicals<sup>60</sup>. The mechanism of formation a radicals and degradation of pollutants is given below.



these photogenerated hydroxyl and peroxy radicals will react with the wattle and degrade them since the wattle is mostly composed of poly phenolic compounds the degradation product may be carbondioxide and mineral acids.

### 3.14 Proposed mechanism

Fig. 16 represents schematic representation of the activity of the mixed oxide catalyst CdWO<sub>4</sub>-ZnO towards wattle degradation and charge carrier separation as explained by Uddin et.al<sup>61</sup>. It is

well known from the literature there is a realignment of Fermi levels when two different phases are mixed together to meet the thermal equilibrium<sup>62</sup>. Here the mixed oxide catalyst is formed with ZnO and CdWO<sub>4</sub>, further it is known the Fermi level of ZnO<sup>63</sup> is higher than that of CdWO<sub>4</sub> hence realignment between the two leads to spontaneous electron transport from ZnO to CdWO<sub>4</sub> which leads to formation of depletion layer and consequently upper bending of band edge occurs. This action altogether eventually drives the formation of a internal electric field. When a visible lamp covering the wavelength range from 400 nm to 760 nm was allowed to shine on the mixed oxide catalyst there is a possibility of creation of electron hole pair in both the metal oxides. The recombination of electron hole pair is prevented by the electric field created at the interface due to formation of heterojunction, furthermore the electrons have the tendency to move towards the electron depleted side therefore there is a vectorial transport of electron in the ZnO semiconductor at the same time there is a hole transport in opposite direction, also it is seen from the diffuse reflectance studies there is a change in band gap value of ZnO at the interface from 3.2 eV to 2.8 eV after mixing with CdWO<sub>4</sub> which makes the catalyst particularly active in visible light. The produced electron and hole diffuse through and reaches the surface of the catalyst and react with the oxygen and water molecules adsorbed over the catalyst to form highly active superoxide radical and activated hydroxy radical respectively, these in turn reacts with the organics in wattle and degrade them into carbon dioxide and mineral acids. A picture of 1% wattle before and after degradation with semiconductor mixed oxide catalyst is also shown in the scheme.

#### 4. Conclusions

A semiconductor mixed oxide catalyst  $\text{CdWO}_4\text{-ZnO}$  was prepared by a simple hydrothermal method. The catalyst had a nanocomposite texture with spheres and flake structure which was also proved with microscopic studies such as SEM and TEM. The chemical composition of the catalyst was analysed with the aid of EDAX, chemical mapping and XPS experiments. The nitrogen adsorption studies prove the mixed oxide catalyst is very porous in nature and seems to have high surface area while comparing to the undoped ZnO. Phase crystallinity of the catalyst has been characterized by XRD studies where the crystallinity and phase purity are evident. The photoluminescence studies flaunted prevention of charge carrier recombination and transfer of charge carriers at the interface of semiconductors. The band gap of the prepared catalyst was determined to be 2.8 eV by using UV-Visible diffuse reflectance spectra. This extension of band gap to visible region by mixing two semiconductive oxides  $\text{CdWO}_4$  and ZnO by means of chemical bond helps the catalyst to work well in the visible region of the spectrum. The catalyst actively degraded the organics of the wattle, a leather tanning agent to an extent of 48% using visible light source, which is a great advantage to the tannery wastewater treating units. Further passing the effluents to the conventional biological treating unit will result in the complete degradation of the pollutants.

### **Acknowledgement**

Financial support from the Council of Scientific and Industrial Research (CSIR), India, under Extra Mural Research (EMR-II) scheme to the project possessing the number GAP - 1401 towards this research work is highly acknowledged.

## 5. References

1. V. Sivakumar, R. P. Prakash, P. G. Rao, B. V. Ramabrahmam and G. Swaminathan, *Journal of Cleaner Production*, 2008, 16, 549-553.
2. IPPC, *European Commission*, 2003.
3. I. Oller, S. Malato and J. A. Sánchez-Pérez, *Science of The Total Environment*, 2011, 409, 4141-4166.
4. G. Farabegoli, A. Carucci, M. Majone and E. Rolle, *Journal of Environmental Management*, 2004, 71, 345-349.
5. G. R. 5. Ramanujam RA, Kandasamy J, *Waste water treatment technology for tanning industry*.
6. M. R. Hoffmann, S. T. Martin, W. Choi and D. W. Bahnemann, *J. Chem. Rev.*, 1995, 95, 69.
7. R. W. Matthews and S. R. McEvoy, *Journal of Photochemistry and Photobiology A: Chemistry*, 1992, 64, 231-246.
8. H. Gerischer, *Electrochimica Acta*, 1993, 38, 3-9.
9. O. Legrini, E. Oliveros and A. M. Braun, *Chemical Reviews*, 1993, 93, 671-698.
10. P. B. Venter, N. D. Senekal, G. Kemp, M. Amra-Jordaan, P. Khan, S. L. Bonnet and J. H. van der Westhuizen, *Phytochemistry*, 2012, 83, 153-167.
11. B. Madhan, C. Muralidharan and R. Jayakumar, *Biomaterials*, 2002, 23, 2841-2847.
12. C. K, *Thesis submitted to University of Madras*, 2014.
13. W. Zheng and S. Y. Wang, *Journal of Agricultural and Food Chemistry*, 2001, 49, 5165-5170.
14. H. F. Stich, *Mutation Research/Genetic Toxicology*, 1991, 259, 307-324.

15. P. K. Mahdi H, Tony C, *Journal of forest products & industries*, 2013.
16. C. Kalyanaraman, S. B. K. Kanchinadham, L. Vidya Devi, S. Porselvam and J. R. Rao, *Industrial & Engineering Chemistry Research*, 2012, 51, 16171-16181.
17. B. Subash, B. Krishnakumar, R. Velmurugan and M. Swaminathan, *Separation and Purification Technology*, 2012, 101, 98-106.
18. D. A. Sobczynski A, *Polish Journal of Environmental Studies*, 2001.
19. Q. Xiang, J. Yu and M. Jaroniec, *Chemical Society Reviews*, 2012, 41, 782-796.
20. M. Nidhin, M. Vedhanayagam, S. Sangeetha, M. S. Kiran, S. S. Nazeer, R. S. Jayasree, K. J. Sreeram and B. U. Nair, *Scientific Reports*, 2014, 4, 5968.
21. H. Zhang, X. Lv, Y. Li, Y. Wang and J. Li, *ACS Nano*, 2010, 4, 380-386.
22. A. L. Linsebigler, G. Lu and J. T. Yates, *Chemical Reviews*, 1995, 95, 735-758.
23. A. P. Alivisatos, *J. Science*, 1996, 271, 933.
24. M. H. Maik E, Christin H, Anna MW, Frank R, Annette T, Robert S, *Angew Chem* 2015, 54, 1.
25. O. K. Kudo A, Kato H *J Am Chem Soc* 1999, 121, 1145.
26. R. Asahi, T. Morikawa, T. Okwaki, K. Aoki and Y. Taga, *Science*, 2001, 293, 269.
27. Z. Zou, J. Ye, K. Sayama and H. Arakawa, *Nature*, 2001, 414, 625-627.
28. M. W. Stoltzfus, P. M. Woodward, R. Seshadri, J.-H. Klepeis and B. Bursten, *Inorganic Chemistry*, 2007, 46, 3839-3850.
29. L. Zhang, W. Wang, J. Yang, Z. Chen, W. Zhang, L. Zhou and S. Liu, *Applied Catalysis A: General*, 2006, 308, 105-110.
30. H. B. Fu, C. S. Pan, W. Q. Yao and Y. F. Zhu, *J. Phys. Chem. B.*, 2005, 109, 22432.
31. S. Klosek and D. Raftery, *The Journal of Physical Chemistry B*, 2001, 105, 2815-2819.

32. P. K. Surolia, R. J. Tayade and R. V. Jasra, *Industrial & Engineering Chemistry Research*, 2007, 46, 6196-6203.
33. A. Fujishima, X. Zhang and D. A. Tryk, *Surface Science Reports*, 2008, 63, 515-582.
34. M.-L. Guan, D.-K. Ma, S.-W. Hu, Y.-J. Chen and S.-M. Huang, *Inorganic Chemistry*, 2011, 50, 800-805.
35. J. Su, X.-X. Zou, G.-D. Li, X. Wei, C. Yan, Y.-N. Wang, J. Zhao, L.-J. Zhou and J.-S. Chen, *The Journal of Physical Chemistry C*, 2011, 115, 8064-8071.
36. H. Lin, H. Ye, S. Chen and Y. Chen, *RSC Advances*, 2014, 4, 10968-10974.
37. W. Wang, X. Huang, S. Wu, Y. Zhou, L. Wang, H. Shi, Y. Liang and B. Zou, *Applied Catalysis B: Environmental*, 2013, 134–135, 293-301.
38. Q.-H. Wu, A. Thißen and W. Jaegermann, *Applied Surface Science*, 2005, 252, 1801-1805.
39. E. W. McFarland and H. Metiu, *Chemical Reviews*, 2013, 113, 4391-4427.
40. R. Liu, H. Ye, X. Xiong and H. Liu, *Materials Chemistry and Physics*, 2010, 121, 432-439.
41. D. Li and H. Haneda, *Journal of Photochemistry and Photobiology A: Chemistry*, 2003, 160, 203-212.
42. Z. Zhang, C. Shao, X. Li, L. Zhang, H. Xue, C. Wang and Y. Liu, *The Journal of Physical Chemistry C*, 2010, 114, 7920-7925.
43. M. T. Uddin, Y. Nicolas, C. Olivier, T. Toupance, L. Servant, M. M. Müller, H.-J. Kleebe, J. Ziegler and W. Jaegermann, *Inorganic Chemistry*, 2012, 51, 7764-7773.
44. S. Lan, L. Liu, R. Li, Z. Leng and S. Gan, *Industrial & Engineering Chemistry Research*, 2014, 53, 3131-3139.

45. D. Ye, D. Li, W. Zhang, M. Sun, Y. Hu, Y. Zhang and X. Fu, *The Journal of Physical Chemistry C*, 2008, 112, 17351-17356.
46. J. L. van Heerden and R. Swanepoel, *Thin Solid Films*, 1997, 299, 72-77.
47. M. Daturi, G. Busca, M. M. Borel, A. Leclaire and P. Piaggio, *The Journal of Physical Chemistry B*, 1997, 101, 4358-4369.
48. V. D. C. S. Ciampi, C. Furlani and G. Polzonetti, *Journal of Electron Spectroscopy and Related Phenomena*, 1992, , 60, 375-383.
49. Y. Zheng, G. Chen, Y. Yu, J. Sun, Y. Zhou and F. He, *RSC Advances*, 2015, 5, 46897-46903.
50. T. Hirakawa and P. V. Kamat, *Journal of the American Chemical Society*, 2005, 127, 3928-3934.
51. N. T. Khoa, S. W. Kim, D.-H. Yoo, S. Cho, E. J. Kim and S. H. Hahn, *ACS Applied Materials & Interfaces*, 2015, 7, 3524-3531.
52. S. Sakthivel and H. Kisch, *Angewandte Chemie International Edition*, 2003, 42, 4908-4911.
53. D. H. E. K. S. W. Sing, R. A. W. Haul, L. Moscou, R. A. Pierotti, J. Rouquerol, T. Siemieniowska, *Pure Appl. Chem*, 1985, 57, 603.
54. T. Sreethawong, Y. Yamada, T. Kobayashi and S. Yoshikawa, *Journal of Molecular Catalysis A: Chemical*, 2005, 241, 23-32.
55. V. Iliev, D. Tomova, L. Bilyarska and G. Tyuliev, *Journal of Molecular Catalysis A: Chemical*, 2007, 263, 32-38.
56. A.-W. Xu, Y. Gao and H.-Q. Liu, *Journal of Catalysis*, 2002, 207, 151-157.

57. A. B. Djurišić, W. C. H. Choy, V. A. L. Roy, Y. H. Leung, C. Y. Kwong, K. W. Cheah, T. K. Gundu Rao, W. K. Chan, H. Fei Lui and C. Surya, *Advanced Functional Materials*, 2004, 14, 856-864.
58. B. Yu, C. Zhu, F. Gan and Y. Huang, *Materials Letters*, 1998, 33, 247-250.
59. M. T. Uddin, Y. Nicolas, C. Olivier, T. Toupance, M. M. Müller, H.-J. Kleebe, K. Rachut, J. Ziegler, A. Klein and W. Jaegermann, *The Journal of Physical Chemistry C*, 2013, 117, 22098-22110.
60. C. D. Zangmeister, S. W. Robey, R. D. van Zee, J. G. Kushmerick, J. Naciri, Y. Yao, J. M. Tour, B. Varughese, B. Xu and J. E. Reutt-Robey, *The Journal of Physical Chemistry B*, 2006, 110, 17138-17144.
61. M. T. Uddin, O. Babot, L. Thomas, C. Olivier, M. Redaelli, M. D'Arienzo, F. Morazzoni, W. Jaegermann, N. Rockstroh, H. Junge and T. Toupance, *The Journal of Physical Chemistry C*, 2015, 119, 7006-7015.
62. M. Mahanti and D. Basak, *RSC Advances*, 2014, 4, 15466-15473.
63. M. G. Samant, *Langmuir*, 1989, 5, 1113-1115.

## Legends and Figures

1. **Fig.1.** images of the mixed oxide catalyst CdWO<sub>4</sub>-ZnO (a) 20KV, (b) 40KV, (c) 80KV magnifications.
2. **Fig. 2.** (a) TEM image of CdWO<sub>4</sub>-ZnO (b) HRTEM of CdWO<sub>4</sub>-ZnO showing the heterojunction of the prepared catalyst (c) SAED pattern of CdWO<sub>4</sub>-ZnO
3. **Fig. 3.** Elemental color mapping of (a) CdWO<sub>4</sub>-ZnO(b) O, (c) Zn, (d) Cd, (e) W, (f) EDAX image of CdWO<sub>4</sub>-ZnO.
4. **Fig. 4.** X-ray diffractogram (a) undoped ZnO, (b) 8.1 wt% of CdWO<sub>4</sub>-ZnO, (c) 23.7 wt% of CdWO<sub>4</sub>-ZnO, (d) 36.8wt% of CdWO<sub>4</sub>-ZnO and (e) CdWO<sub>4</sub>
5. **Fig. 5.** (a) XPS showing the survey scan for the mixed oxide catalyst CdWO<sub>4</sub>-ZnO (b) shows the high resolution peak for adventitious carbon.
6. **Fig.6.** XPS Showing the high resolution peak for (a) cadmium (b) tungsten (c) Zinc (d) Oxygen, with the orbital splitting peaks.
7. **Fig. 7.** AFM images CdWO<sub>4</sub>-ZnO (a) surface topography of 3 μm x 3 μm region (b) 3D view
8. **Fig. 8.** Photoluminescence Spectra (a) undoped ZnO and (b) CdWO<sub>4</sub>- ZnO
9. **Fig. 9.** N<sub>2</sub> adsorption-desorption isotherm of CdWO<sub>4</sub>-ZnO
10. **Fig. 10.** Diffuse reflectance spectra of (a) Bare ZnO and (b) CdWO<sub>4</sub>-ZnO catalyst
11. **Fig. 11.** IR spectroscopy images of wattle extract (a) before and (b) after degradation
12. **Fig. 12.** Plot showing the degradation of wattle in terms of reduction in % of COD versus time with 50, 100 and 150 mg of mixed oxide catalyst ZnO-CdWO<sub>4</sub>,
13. **Fig. 13.** Plot showing the degradation of wattle in terms of reduction in % of COD versus time with 50, 100 and 150 mg of undoped ZnO
14. **Fig.14.** showing the plots of C/C<sub>0</sub> versus time (a) for different amount of mixed oxide catalyst CdWO<sub>4</sub>-ZnO and (b) for different amount of ZnO catalyst.

15. **Fig 16.** Display of ESR signal for (a) ZnO (b) ZnO after UV shine (c) CdWO<sub>4</sub> - ZnO (d) CdWO<sub>4</sub> – ZnO after UV shine.
16. **Fig.15.** Schematic representation showing the charge separation and mechanism of photocatalytic degradation of wattle

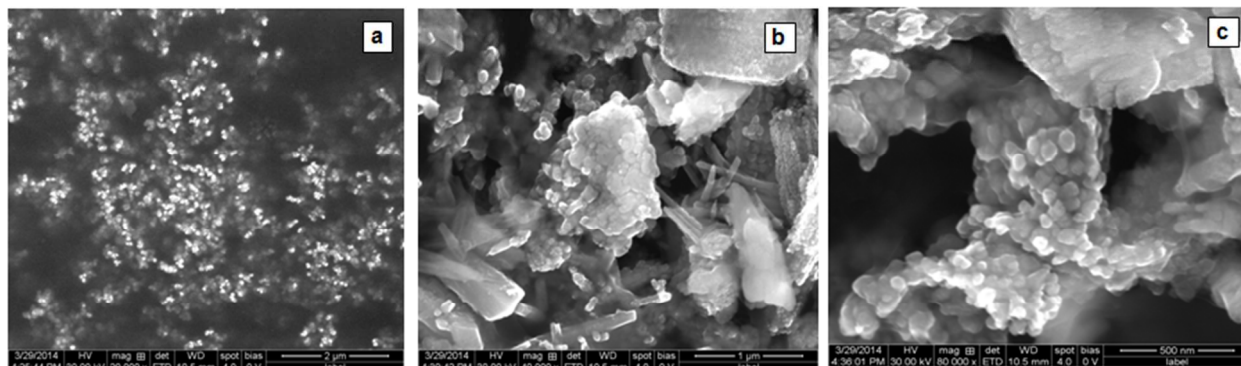


**Fig. 1.** FESEM images of the mixed oxide catalyst CdWO<sub>4</sub>-ZnO (a) 20KV, (b) 40KV, (c) 80KV magnifications.

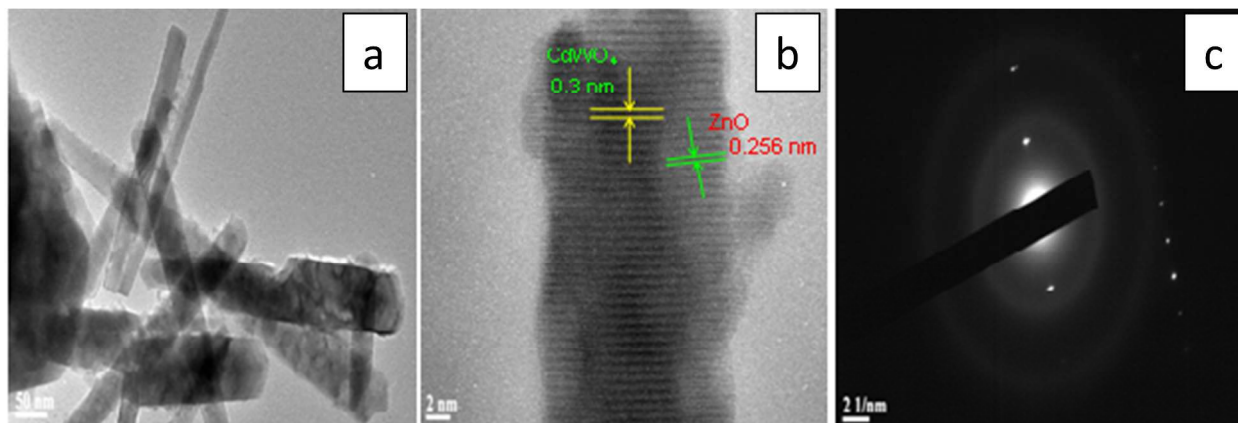


**Fig. 2.** (a) TEM image of CdWO<sub>4</sub>-ZnO (b) HRTEM of CdWO<sub>4</sub>-ZnO showing the heterojunction of the prepared catalyst (c) SAED pattern of CdWO<sub>4</sub>-ZnO

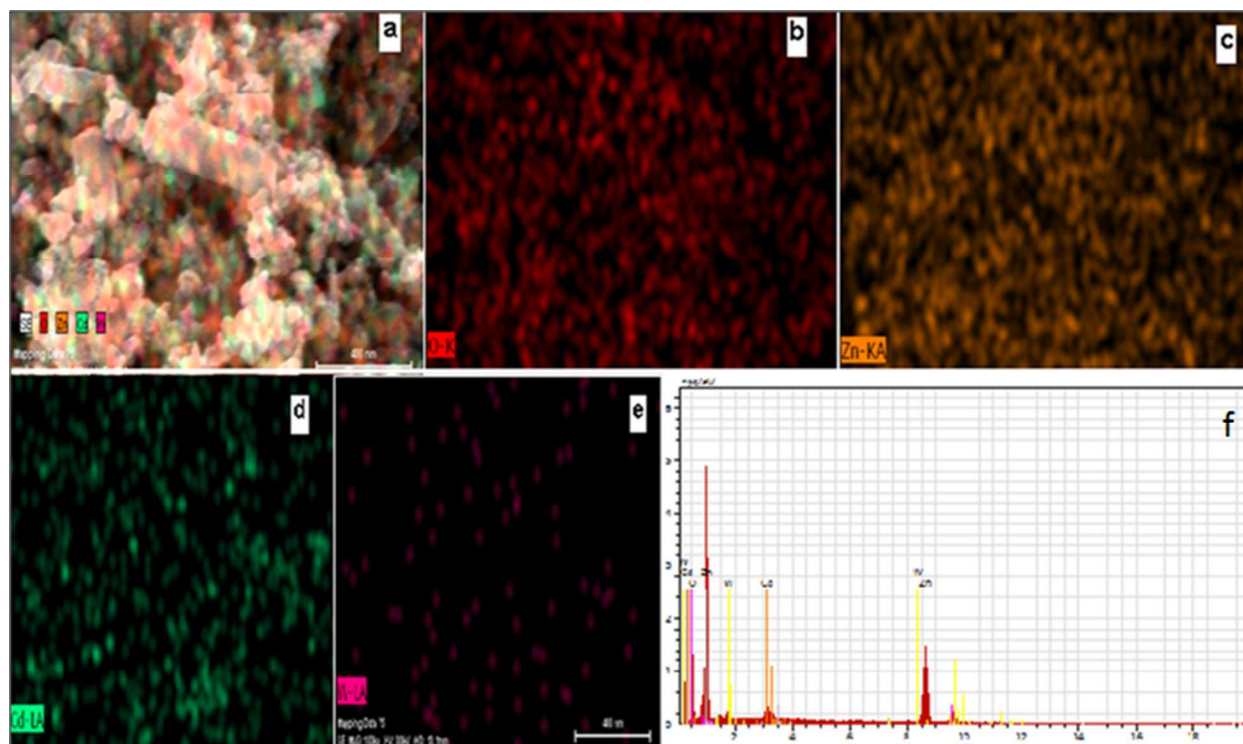


**Fig. 3.** Elemental color mapping of (a)  $\text{CdWO}_4\text{-ZnO}$  (b) O, (c) Zn, (d) Cd, (e) W, (f) EDAX image of  $\text{CdWO}_4\text{-ZnO}$ .

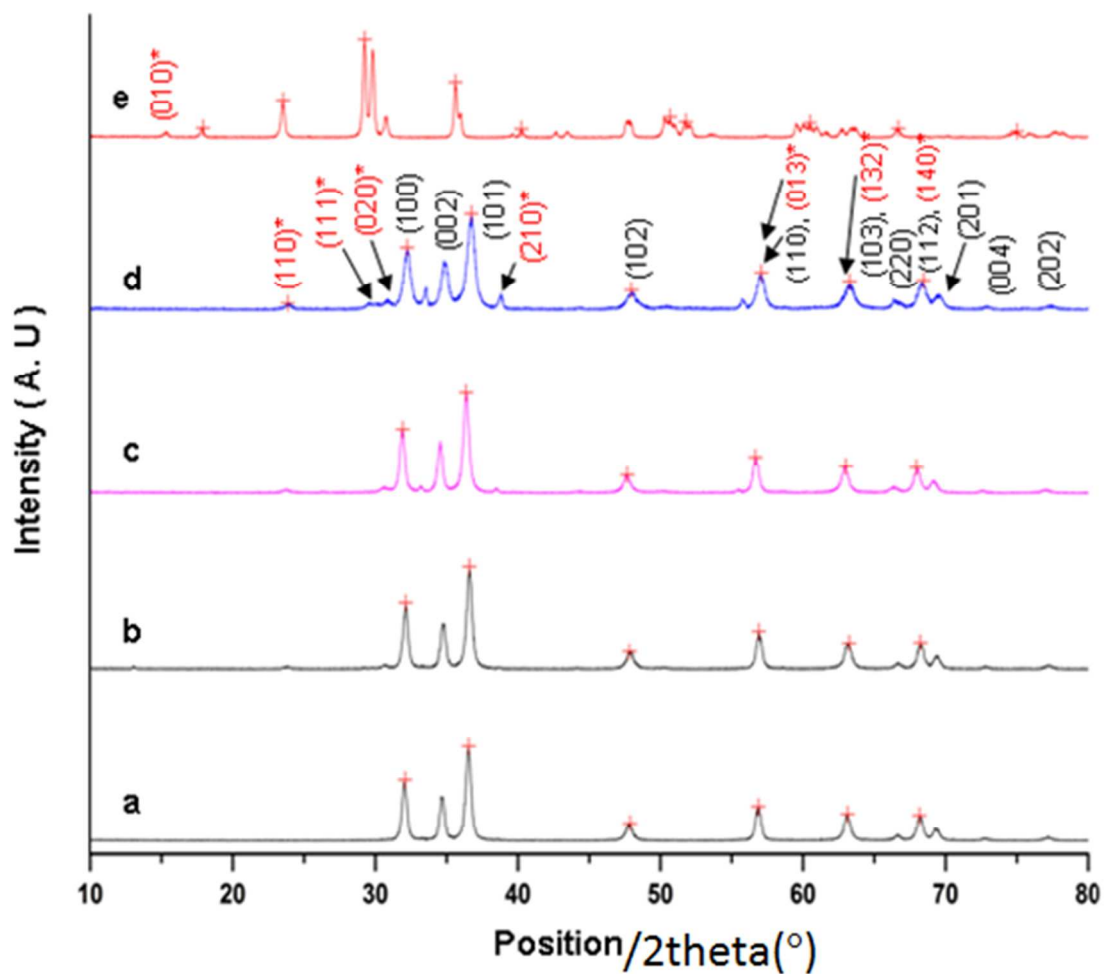


**Fig. 4.** X-ray diffractogram (a) undoped ZnO, (b) 8.1 wt% of CdWO<sub>4</sub>-ZnO, (c) 23.7 wt% of CdWO<sub>4</sub>-ZnO, (d) 36.8wt% of CdWO<sub>4</sub>-ZnO and (e) CdWO<sub>4</sub>

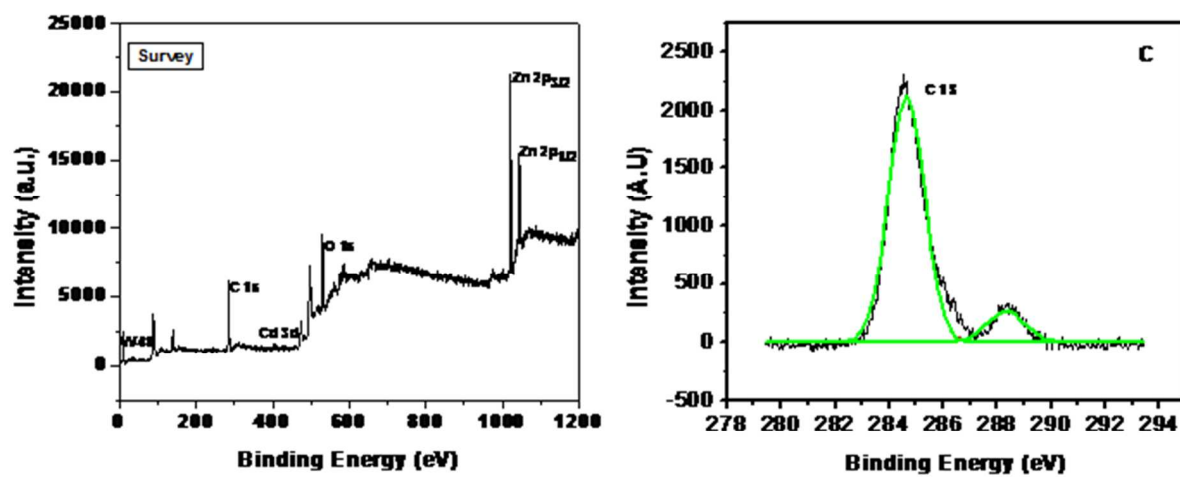


**Fig. 5.** (a) XPS showing the survey scan for the mixed oxide catalyst CdWO<sub>4</sub>-ZnO (b) shows the high resolution peak for adventitious carbon.

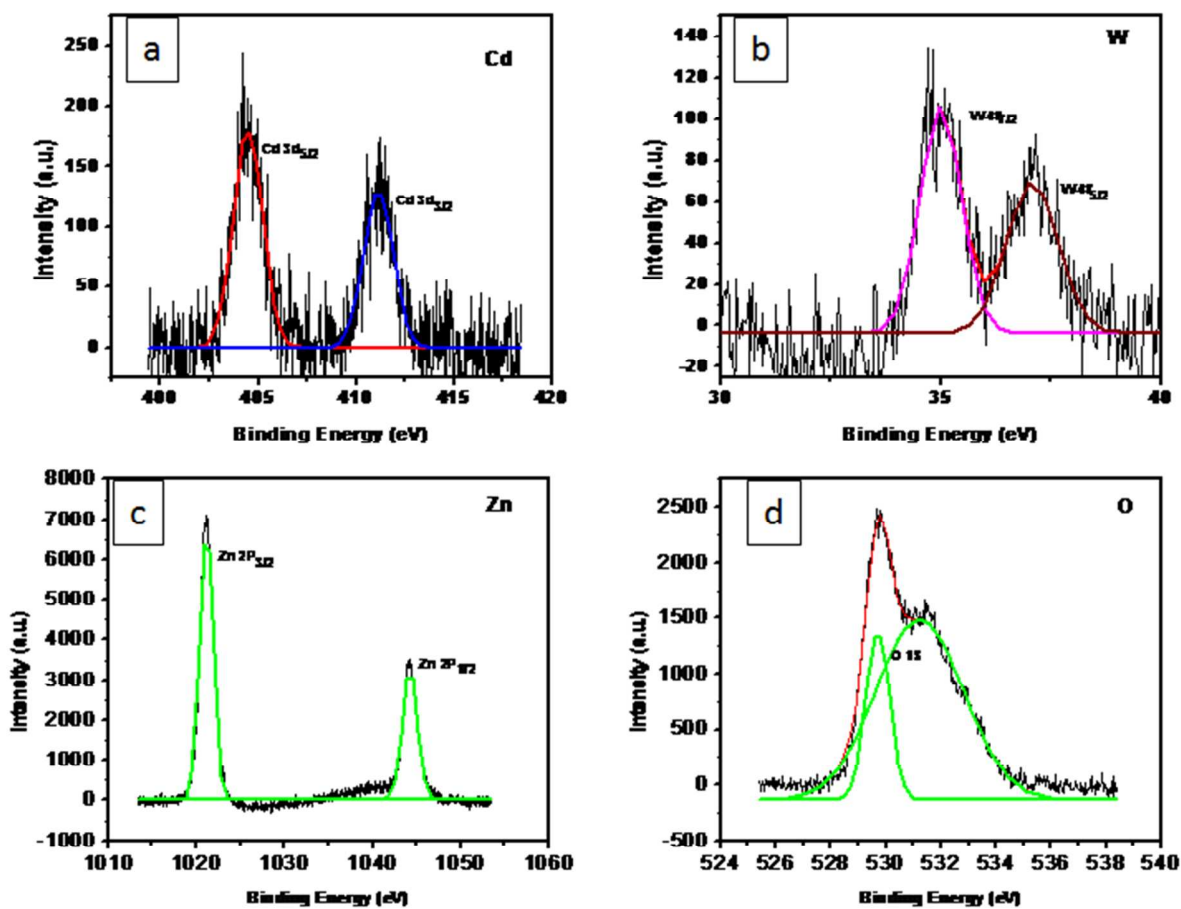
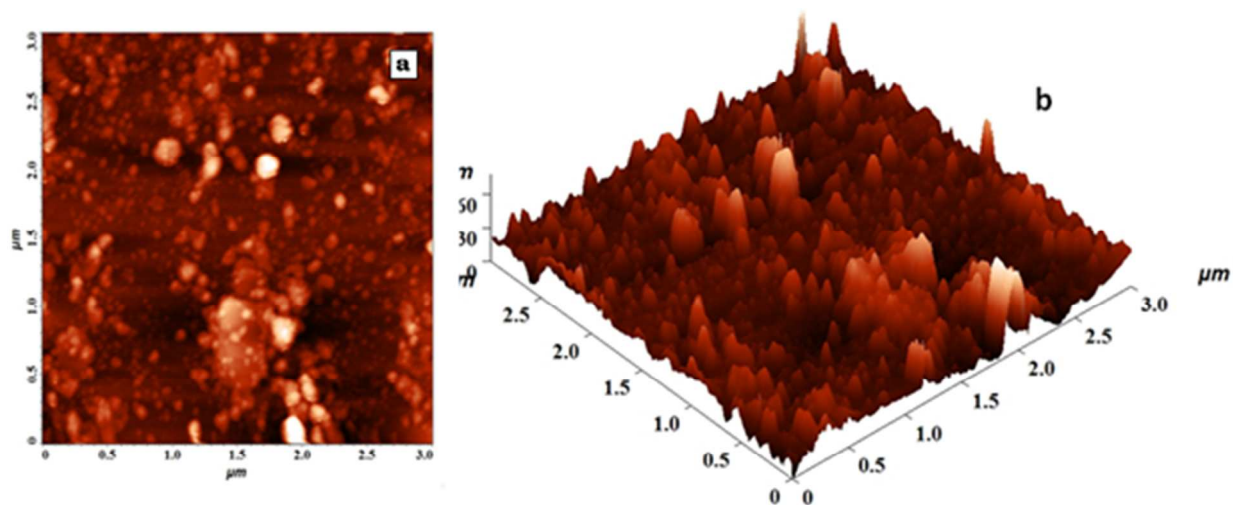
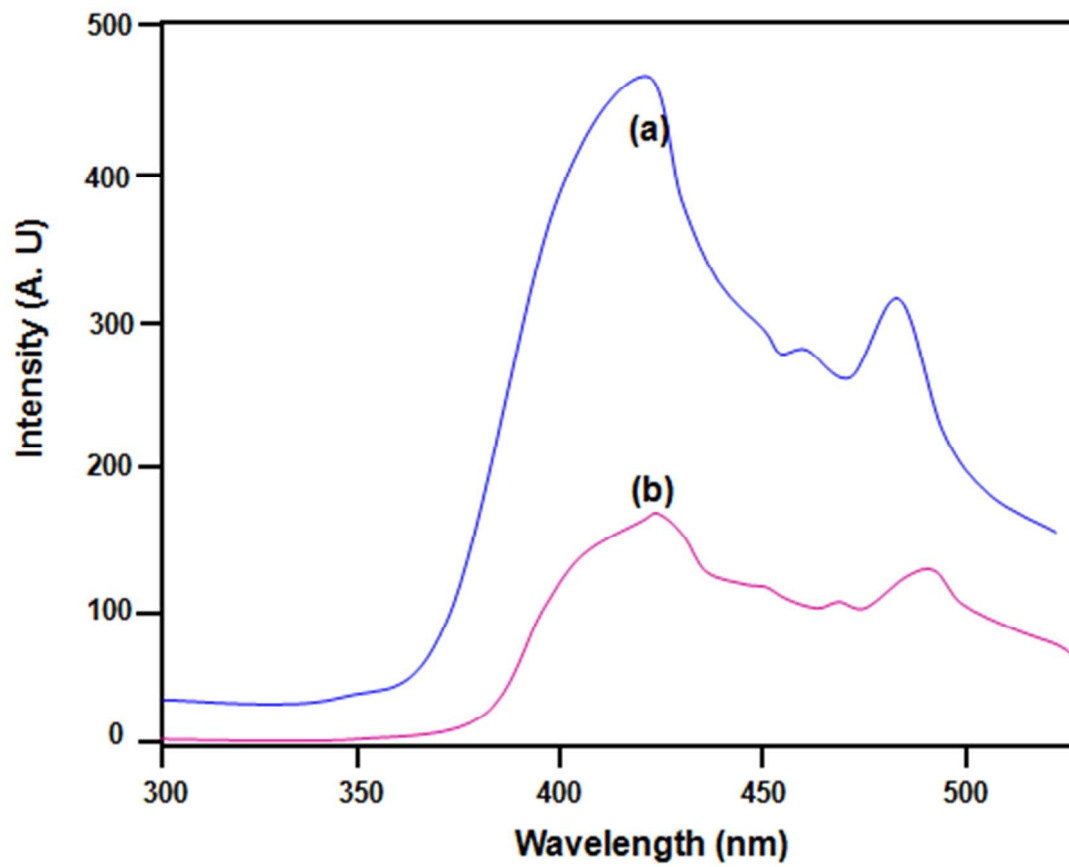


Fig.6. XPS Showing the high resolution peak for (a) cadmium (b) tungsten (c) Zinc (d) Oxygen, with the orbital splitting peaks.



**Fig. 7.** AFM images CdWO<sub>4</sub>-ZnO (a) surface topography of 3 μm x 3 μm region (b) 3D view



**Fig. 8.** Photoluminescence Spectra (a) undoped ZnO and (b) CdWO<sub>4</sub>-ZnO

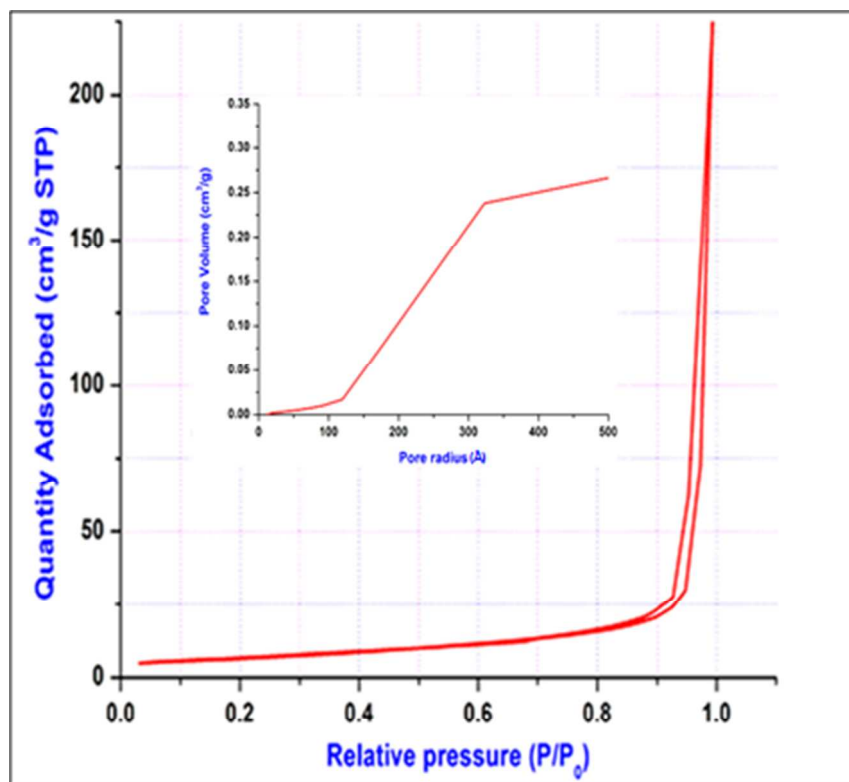
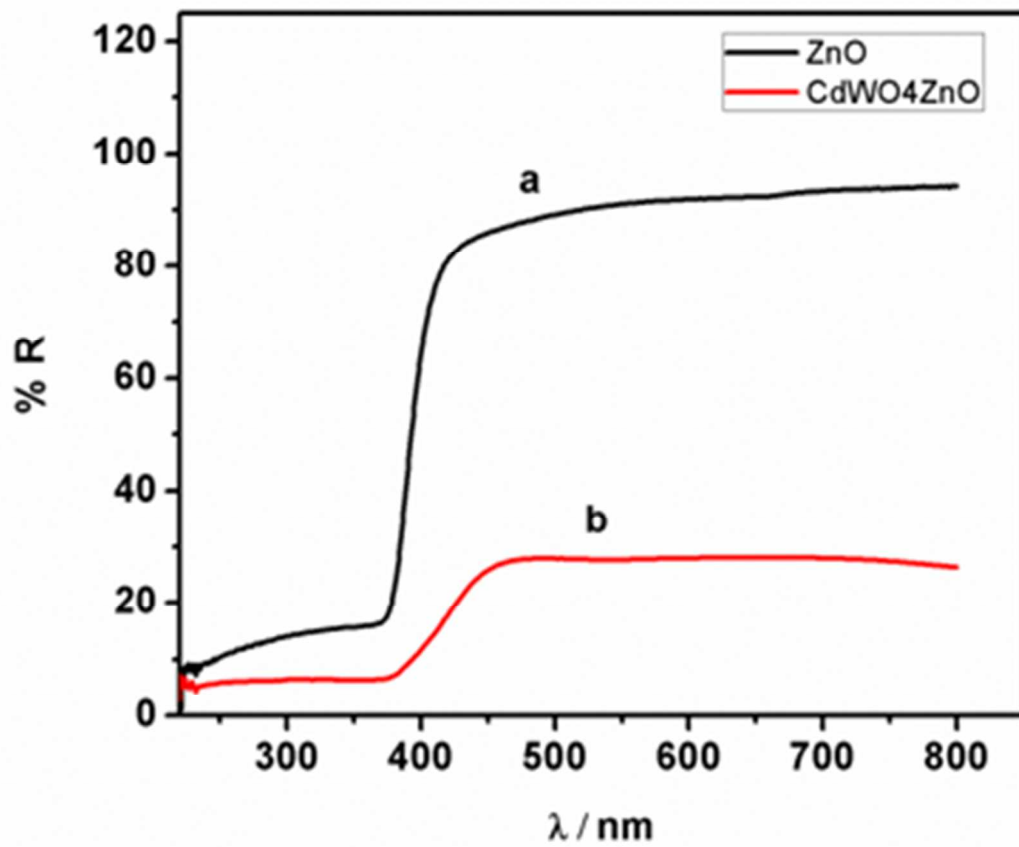
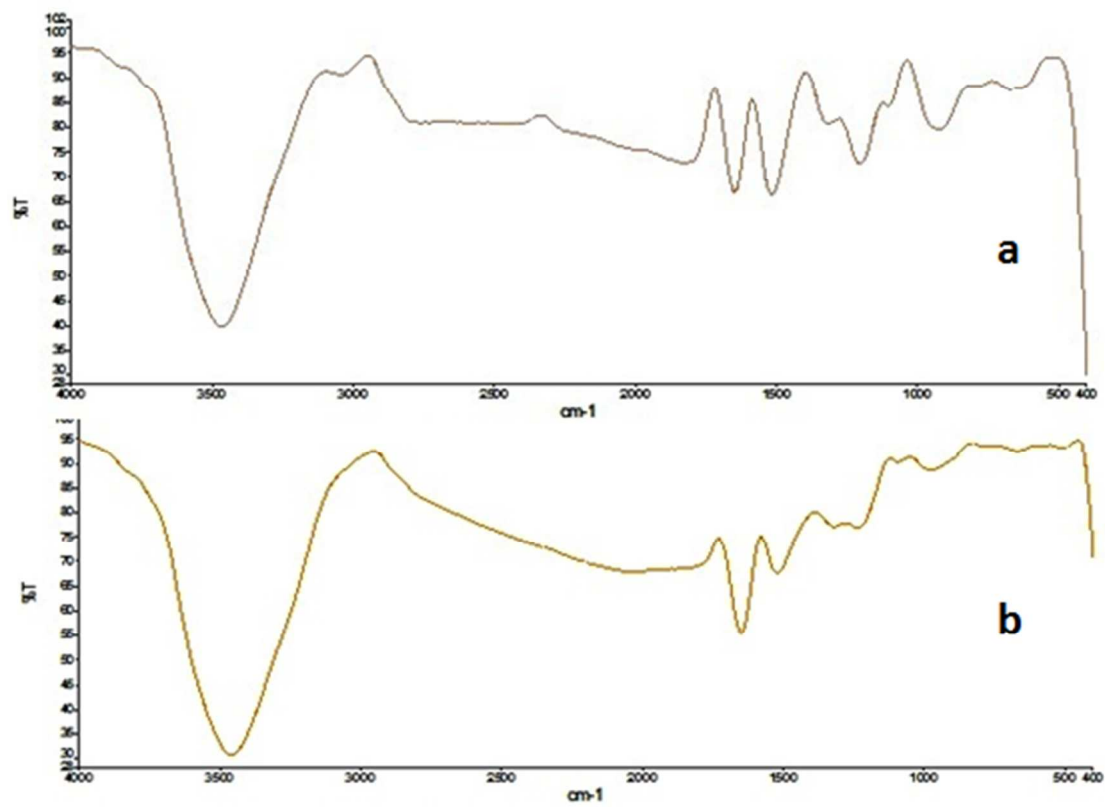


Fig. 9. N<sub>2</sub> adsorption-desorption isotherm of CdWO<sub>4</sub>-ZnO





**Fig. 10.** Diffuse reflectance spectra of (a) Bare ZnO and (b) CdWO<sub>4</sub>-ZnO catalyst



**Fig. 11.** IR spectroscopy images of wattle extract (a) before and (b) after degradation

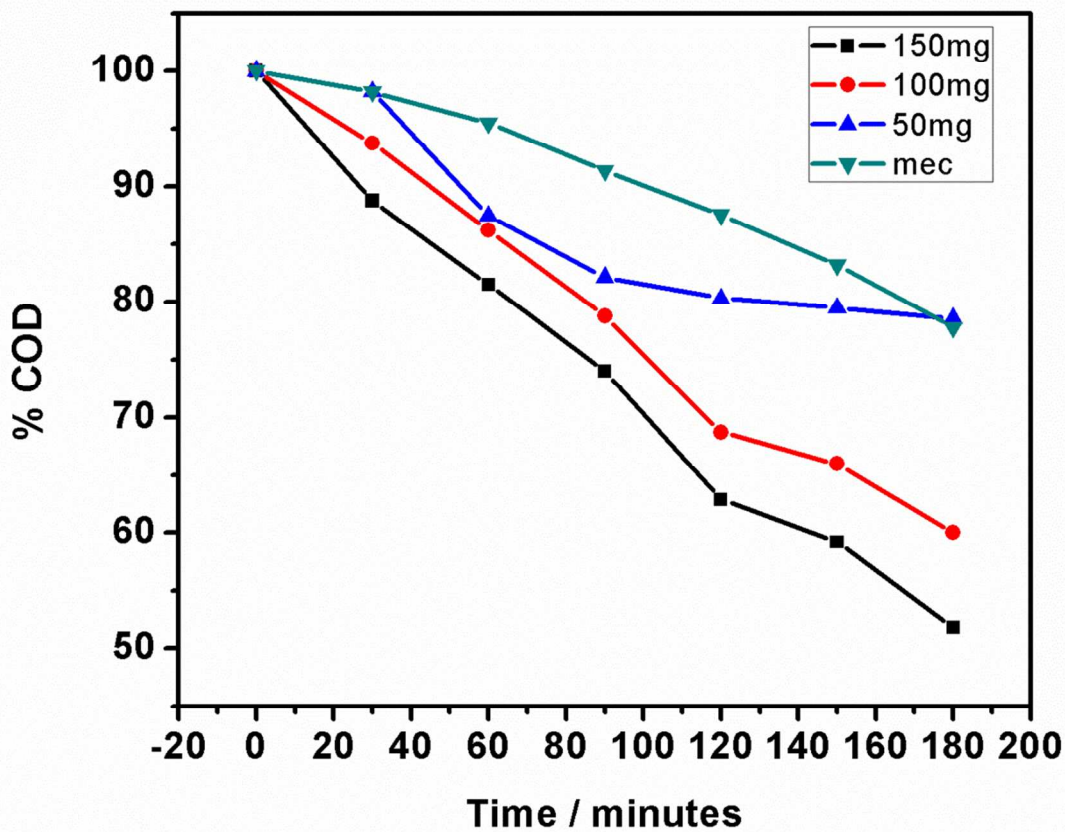


**Fig. 12.** Plot showing the degradation of wattle in terms of reduction in % of COD versus time with 50, 100 and 150 mg of mixed oxide catalyst ZnO-CdWO<sub>4</sub>, green colour plot shows the COD plot for mechanical mixing of ZnO and CdWO<sub>4</sub> semiconductors.

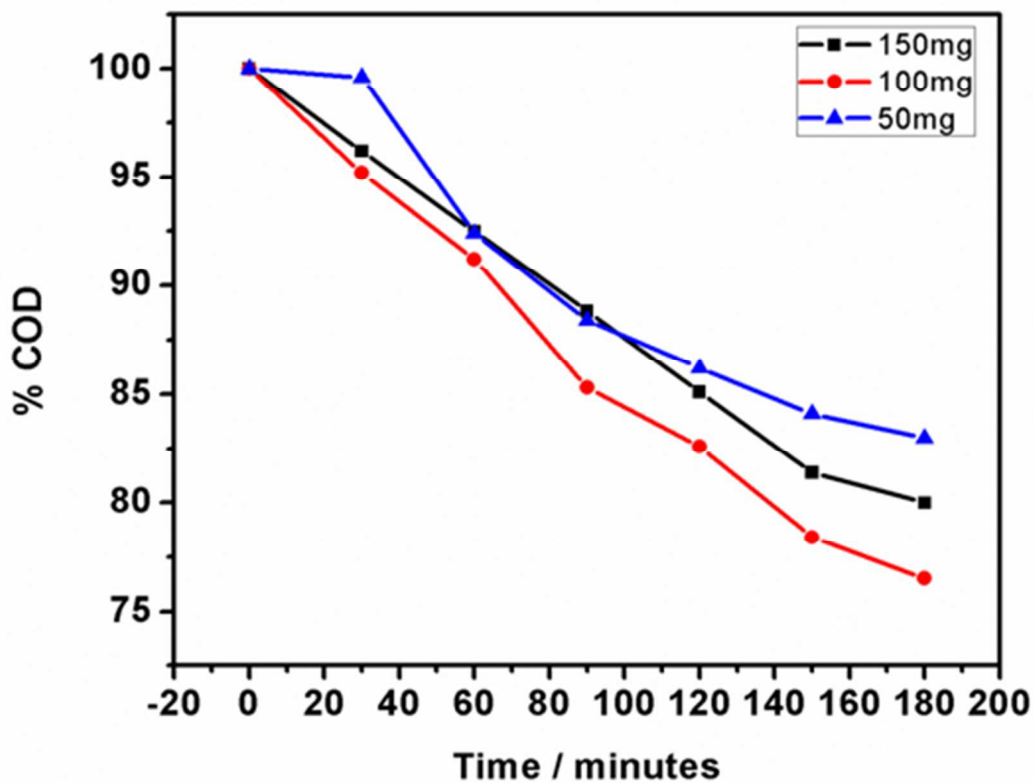


**Fig. 13.** Plot showing the degradation of wattle in terms of reduction in % of COD versus time with 50, 100 and 150 mg of undoped ZnO

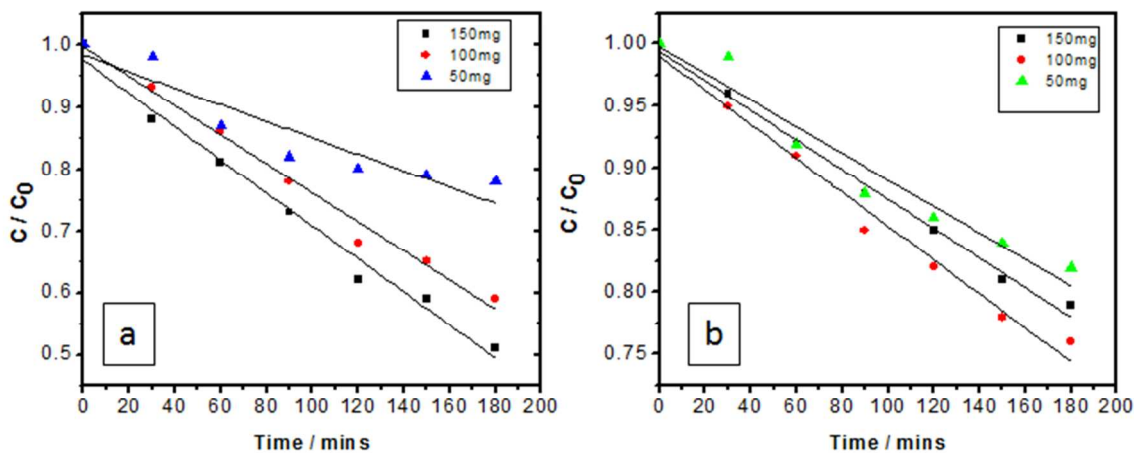


**Fig.14.** showing the plots of  $C/C_0$  versus time (a) for different amount of mixed oxide catalyst  $CdWO_4-ZnO$  and (b) for different amount of  $ZnO$  catalyst.

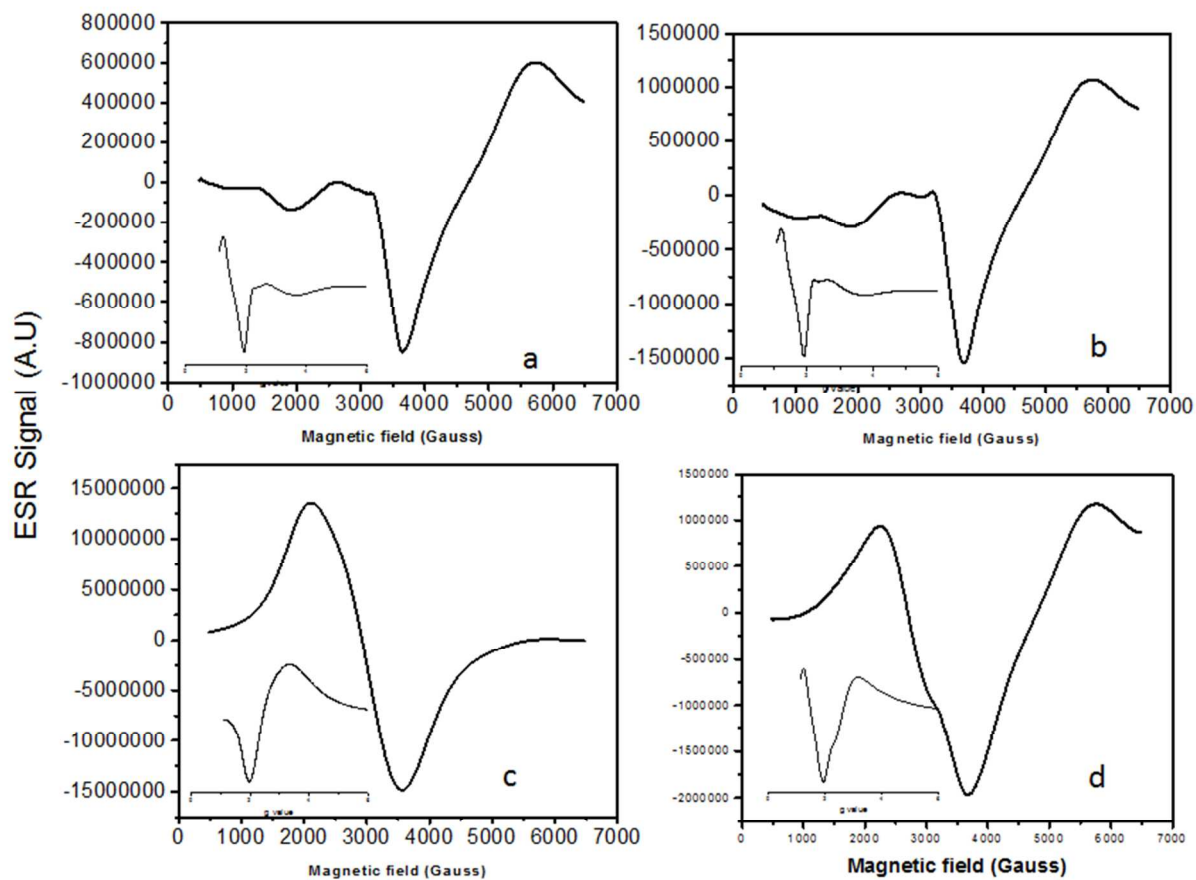


**Fig 15.** Display of ESR signal for (a)  $ZnO$  (b)  $ZnO$  after UV shine (c)  $CdWO_4 - ZnO$  (d)  $CdWO_4 - ZnO$  after UV shine.

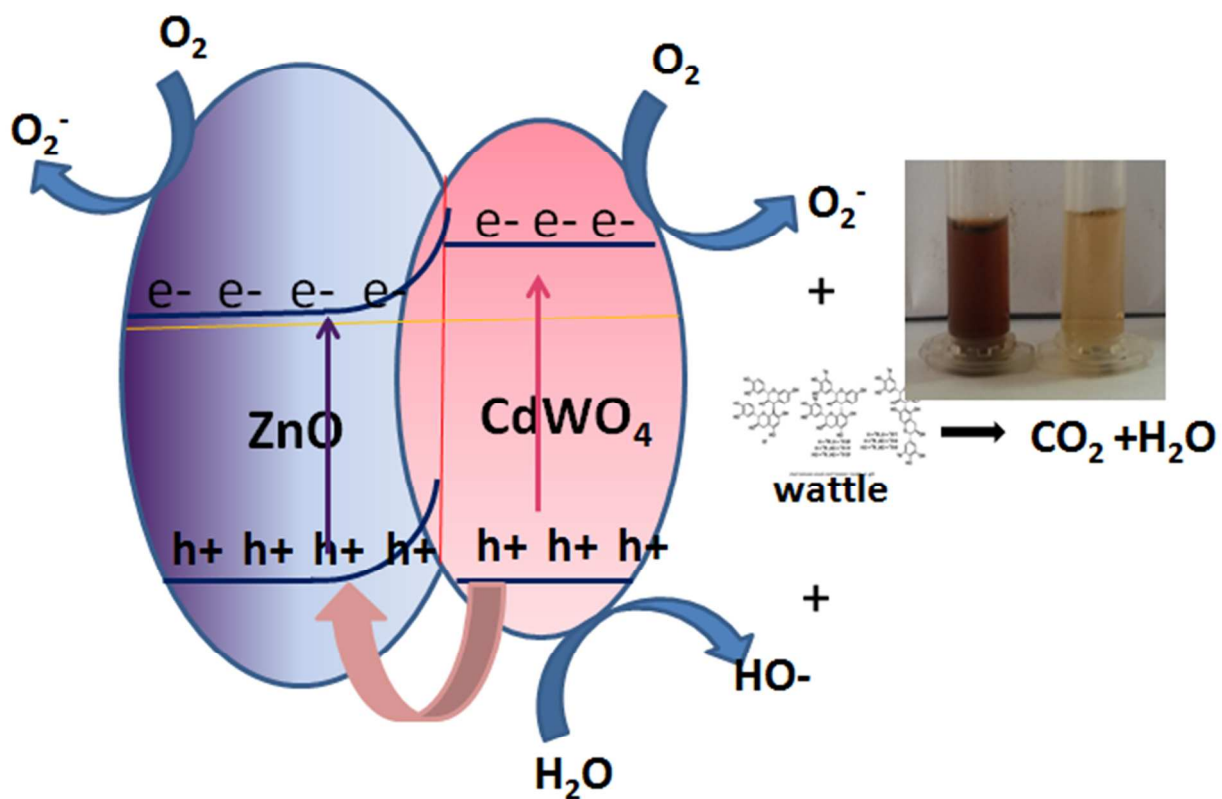


**Fig.16.** Schematic representation showing the charge separation and mechanism of photocatalytic degradation of wattle